Fault-Tolerant Field-Oriented Control of Three-Phase Induction Motor Based on Unified Feedforward Method

Mahdi Tousizadeh, Hang Seng Che, *Member, IEEE*, Jeyraj Selvaraj, Nasrudin Abd Rahim, *Senior Member, IEEE*, and Boon-Teck Ooi, *Life Fellow, IEEE*

***Abstract*—With the increasing proliferation of variable speed drive, the demand for the more reliable drive is also on the rise. Despite the growing interest on more advanced motors like permanent magnet and flux switching motors, three-phase induction motors (3ph-IMs) are still the main workhorse in the industry and hence the fault-tolerant control of these motor drives remains an interesting and important topic. In this paper, a simple fault-tolerant field-oriented control technique for 3ph-IMs is presented. It is shown that by injecting zero-sequence compensation voltage in a feedforward manner, open-circuit faults can be effectively tolerated. Compared to the previous feedforward fault-tolerant control methods, the proposed approach does not require the knowledge of the magnetizing inductance, which is tricky to be obtained in induction motors. Furthermore, the unified feedforward approach allows the same control structure to be used for different fault-tolerant 3ph-IMs drive topologies, with minor modifications to the feedforward terms. In addition, the effect of inverter non-idealities on the performance of the proposed control method is also highlighted and addressed. The effectiveness of the proposed controller is verified using MATLAB simulation and further validated using experimental tests. This paper is accompanied by a video demonstrating the experimental results.**

***Index Terms*—Fault-tolerant drive, induction motor (IM), post-fault, reliability, three-phase ac motor drive.**

I. Introduction

DUE to its low cost, robustness, and construction simplicity, induction motors (IMs) have found widespread usage in various industries over the years. With the advancement in power electronics technology, the usage of IMs particularly three-phase IMs has been further enhanced, finding their place in

Manuscript received July 16, 2018; revised September 5, 2018; accepted November 17, 2018. Date of publication December 3, 2018; date of current version May 22, 2019. This work was supported by the Malaysian Ministry of Higher Education under Project MO013-2016. Recommended for publication by Associate Editor J. Hur. *(Corresponding author: Hang Seng Che.)*

M. Tousizadeh, H. S. Che, J. Selvaraj, and N. A. Rahim are with the Power Energy Dedicated Advanced Centre, University of Malaya, Kuala Lumpur 59990, Malaysia (e-mail:

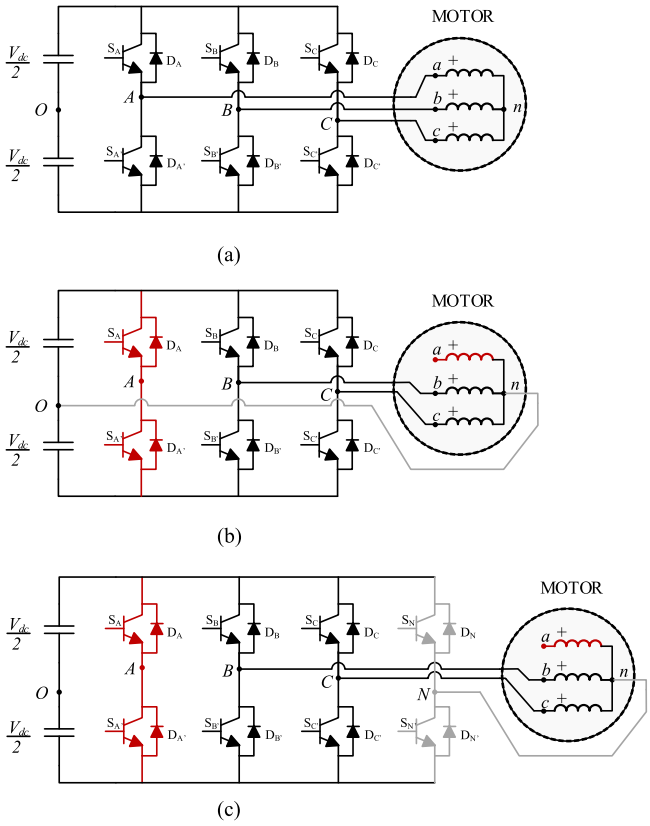

Fig. 1. Three-phase drive in (a) healthy mode and post-fault mode. (b) Neutral to capacitor midpoint, 3 L-NCM. (c) Neutral to auxiliary leg, (3 + 1)L-NAL topology, with two active phases remaining.

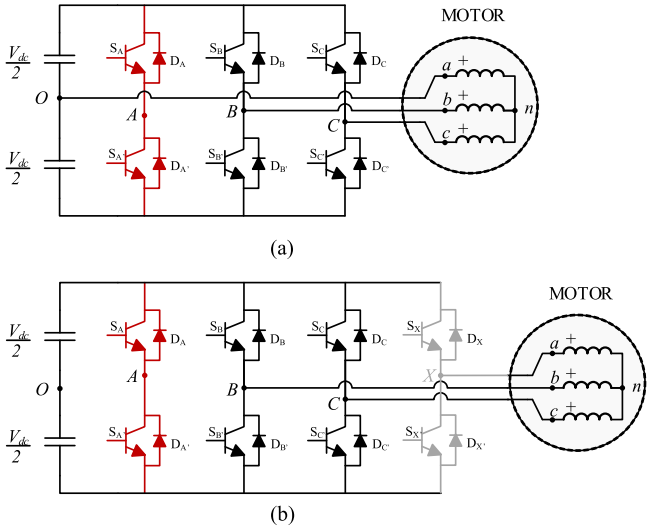

Fig. 2. Post-fault topology. (a) Phase to capacitor midpoint, 3 L-PCM. (b) Phase to auxiliary leg, (3 + 1)L-PAL topology, with three active phases remaining.

as 3-legs inverter with faulted phase connect to capacitor midpoint (3L-PCM) [see Fig. 2(a)] and 3 + 1 legs inverter with faulted phase connected to additional leg (3 + 1) L-PAL [see Fig. 2(b)], respectively. These topologies allow the motor to operate with three phases even after fault, with minimal control reconfiguration.

However, the post-fault machine will have to run as a "two-phase motor" if one of the motor phases is disabled due to the fault. For a wye-connected 3ph-IM, the requirement to achieve such fault tolerance is to provide a path for the neutral current to flow [1], [2], [10]–[14]. This neutral current can be circulated back to the dc link, either via capacitor midpoint in 3 L-NCM configuration [see Fig. 1(b)], or through an auxiliary inverter leg for the (3 + 1)L-NAL topology [see Fig. 1(c)]. Furthermore, the reconfiguration of the drives must be accompanied with appropriate modifications to the controller in order for the motor to resume proper operation. Since the machine is no longer a balanced three-phase machine, the fault-tolerant control of IM under 3 L-NCM and (3 + 1)L-NAL topologies are more challenging and has been the subject of various studies in the past.

Between the two, the 3 L-NCM approach is favored for its simplicity but suffers from the dc-link midpoint voltage oscillation problem which can cause voltage/current distortions and requires increase dc-link capacitors. Various works have been dedicated to mitigate this issue by phase asymmetric pulsewidth modulation (PWM) technique [1] or hardware-based solutions with field-oriented control (FOC) [2].

Several works on fault-tolerant control of (3 + 1)L-NAL configuration have been reported in the literature. In [12], double synchronous reference frame PI controllers were proposed with (3 + 1)L-NAL topology with good steady-state performance. In [10] and [11], the authors demonstrated a simple feedforward fault-tolerant control method for a three-phase permanent magnet synchronous motor (PMSM) based on the conventional synchronous PI FOC method. By calculating the correct compensation voltages and adding them to the synchronous PI FOC controller outputs in feedforward manner, the fault-tolerant control of the three-phase PMSM drive can be achieved. The sensorless extension of [10] with a closed-loop filed weakening controller is given in [14] to further increase the reliability. In [13], an innovative PMSM model with appropriate reference frame transformation treats a faulted drive similar to the healthy one under vector control.

From the literature reviewed, the following points can be highlighted.

1) Fault-tolerant control methods for 3ph-IM drives have always been discussed separately and are specific to the configuration of the fault-tolerant drive topology.
2) The feedforward method in [10] and [11] requires accurate knowledge on rotor flux, which can be tricky when extended from PMSM to IM, since this requires accurate knowledge on the magnetizing inductance.
3) For the feedforward method, the effect of inverter nonlinearities is expected to be detrimental to the accuracy of the compensation voltage, but this was not discussed in prior studies.

In this paper, a general fault-tolerant FOC strategy for 3ph-IM drive, suitable for all four configurations in Figs. 1 and 2, has been proposed. Using a unified feedforward compensation method, OPF can be compensated for different drive topologies while maintaining the original FOC structure.

Discussions in subsequent parts of this paper are structured in the following manner: Section II provides theoretical analysis on

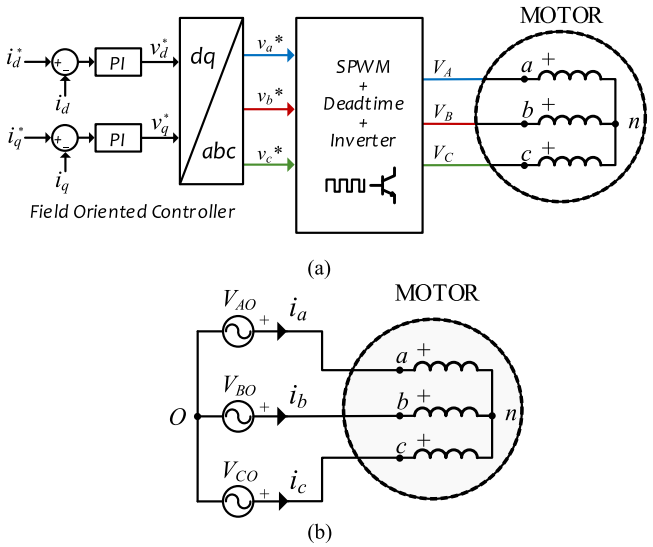

Fig. 3. Schematic of FOC current controller and the equivalent circuit diagram of drive in healthy operation.

the 3ph-IM in healthy and faulty modes, with focus being given to the operation of the faulty drive with only two active phases remaining. Here, the use of zero-sequence voltage injection to compensate the fault is explained. In Section III, the method of determining zero-sequence voltage is presented, followed by discussion on inverter nonlinearities and their compensation in Section IV. Finally, the simulation and experimental results are provided to validate the effectiveness of the proposed fault-tolerant FOC method.

II. Healthy and Faulted IM Under FOC

A. Healthy Operation of IM Drive

The FOC of 3ph-IM is based on the projection of three-phase current, voltage, and fluxes of the IM onto a two-dimensional (dq) plane, using Clarke and Park transformations. This technique allows the torque and flux currents to be controlled as separate dc quantities using simple PI controllers, before converting the control voltages back into ac signals. Fig. 3(a) illustrates the simplified relations between the key components in a 3ph-IM drive with inverter topology shown in Fig. 1(a).

As seen in Fig. 3(a), the inverter pole voltages (w.r.t to dc-link midpoint), V_{AO}, V_{BO}, and V_{CO} are directly proportional to the control variables v_a^*, v_b^*, and v_c^* if sinusoidal pulsewidth modulation (SPWM) is utilized. So, the phase voltage applied to the motor is indirectly defined through inverter pole voltage. For healthy operation under FOC, the inverter could be represented as three controlled voltage source V_{AO}, V_{BO}, and V_{CO}, as shown in Fig. 3(b) where the voltage source inverter is used.

In healthy case, both the control voltages v_a^*, v_b^*, and v_c^* (which are the same as V_{AO}, V_{BO}, and V_{CO}) and phase currents are balance three-phase quantities, which appear as dc components on dq plane.

As a result, effective control can be achieved using PI controllers. However, this scenario is not valid for a faulted drive due to disruption in relation between inverter pole voltage and phase voltage applied to the motor.

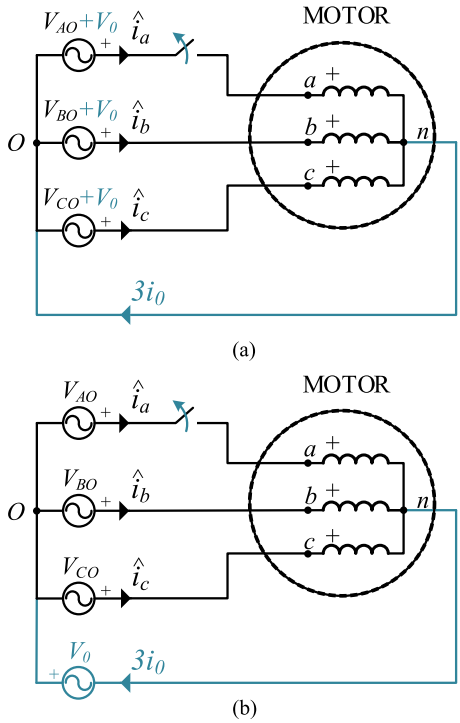

Fig. 4. Three-phase drives with capability of injecting zero-sequence current.

B. Faulted Drive With Two Active Phases

In case of OPF, the topology of the reference healthy drive shown in Fig. 1(a) should be modified to Fig. 1(b) or (c). To ensure the drive capability, the relation between motor phase voltages and inverter pole voltages (i.e., the control voltages) has to be reconsidered due to: 1) changes in phase currents; and 2) topology reconfiguration.

As discussed in [10], the unbalanced two-phase machine resulted in dc + ac d–q control voltages, which are beyond the control capability of the PI controllers, causing deteriorated control performance. However, if the "disturbance" ac voltages can be compensated, the PI controllers will only require to generate the dc d–q control voltages and the fault-tolerant control of the machine can be attained. This can be done by injecting suitable zero-sequence voltage(s), such that zero-sequence current can be injected compensating the OPF. There are two ways to achieve this depending on the converter topology, which are explained subsequently with the aid of Fig. 4.

Now, assume that there is a path for the motor neutral current to return to the inverter, as shown in Fig. 4(a), and the machine is operating with balanced three-phase voltages and currents. A zero-sequence voltage can be added to the inverter pole voltages, such that $i_0 = -i_a$ and the new phase currents become

$$i_0 = -i_a \Rightarrow \hat{i}_a = i_a - i_a = 0,\ \hat{i}_b = i_b - i_a,\ \hat{i}_c = i_c - i_a \tag{1}$$

where the hat symbols represent the post-fault quantities.

Since the current in phase "*a*" is zero, its phase connection can be open circuited without affecting the performance of the machine. This essentially resulted in the same scenario as a 3ph-IM with OPF in phase "*a*".

Based on the concept of superposition, a faulted 3ph-IM with two active phases and a neutral return path can be considered as the superposition of a healthy balanced 3ph-IM (supply balance i_a, i_b, and i_c) with a zero-sequence circuit (supplying $i_0 = -i_a$). If zero-sequence current can be correctly injected via feedforward zero-sequence voltage, the synchronous PI controller will be able to control the remaining "healthy" machine and fault-tolerant control can be achieved without changing the controller structure.

This idea is realizable if and only if there is a path for zero-sequence current to flow. There are two ways to accommodate the flow of zero-sequence current and different ways of applying zero-sequence voltage.

1) 3 L-NCM topology in Fig. 1(b): the motor neutral is connected directly to the capacitor midpoint, with the equivalent circuit as shown in Fig. 4(a). Zero-sequence voltage has to be added to all three inverter pole voltages, as shown in the figure.
2) (3 + 1)L-NAL configuration in Fig. 1(c): the motor neutral is connected to an auxiliary inverter leg, giving an equivalent circuit as shown in Fig. 4(b). In this case, zero-sequence voltage can be injected by directly providing V_0 at the auxiliary leg.

From control perspective, the injection of the zero-sequence voltage can be done by

1) 3 L-NCM topology: adding V_0 to the three control voltages v_a^*, v_b^*, and v_c^* in a feedforward manner;
2) (3 + 1)L-NAL topology: using V_0 as the control voltages for the axillary leg in a feedforward manner.

From Fig. 4, it is obvious that regardless of the configuration, the same zero-sequence voltage V_0 is required. Since feedforward compensation is utilized, it is important to determine the correct voltage required to create the correct zero-sequence current.

III. Determination of Zero-Sequence Voltage

A. Zero-Sequence Parameters of an IM

The ideal zero-sequence model for 3ph-IM contains the stator resistance in series with stator leakage inductance $(R_s + jX_{ls})$ without flux-linkage path between stator and rotor windings [23]. However, due to the physical arrangement of the stator winding, the instantaneous modular multilevel converter (MMF) produced by zero-sequence current at an electrical angle of θ (w.r.t. any stator phase winding) at time t and the synchronous electrical speed of ω_s is actually given by

$$\begin{aligned}&\mathrm{MMF}_n(\theta)\\&= K_n F_n \left(1 + 2\cos\frac{2n\pi}{3}\right)\cos\left(n\theta + \frac{2n\pi}{3}\right)\sin(\omega_s t)\end{aligned} \quad (2)$$

where the parameters K_n and F_n are the harmonic winding factor and the amplitude of nth harmonic, respectively. Hence, for stator winding coil span other than two-third the pole pitch,

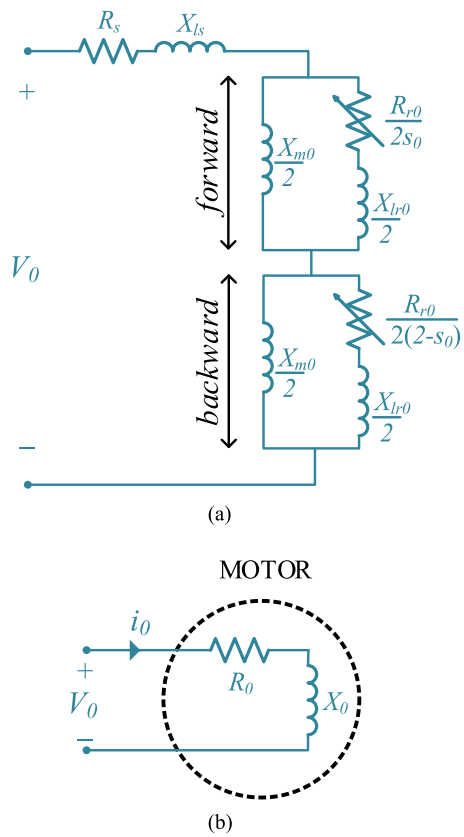

Fig. 5. Zero-sequence model of a 3ph-IM. (a) Complete model. (b) Equivalent circuit.

the flow of zero-sequence current can create third and multiples of third MMF harmonics that couples with the rotor, with the harmonics higher than the third usually negligible [24], [25].

It has been further demonstrated that this resultant magnetic field in airgap is pulsating similar to a single phase IM, but at one-third of the forward-rotating frequency, i.e., $\omega_0 = \omega_s/3$. Based on the double revolving field theory commonly used for a single-phase machine, the equivalent circuit for this zero-sequence circuit is shown in Fig. 5(a).

The rotor parameters are involved in total zero-sequence impedance, as demonstrated in Fig. 5(a) and it could be lumped together as shown in Fig. 5(b)

$$\begin{aligned}R_0 + jX_0 &= R_{s0} + jX_{ls0}\\&\quad + jX_{m0}/2\left(\frac{jX_{lr0} + R_{r0}/s_0}{jX_{m0} + jX_{lr0} + R_{r0}/s_0}\right)\\&\quad + jX_{m0}/2\left(\frac{jX_{lr0} + R_{r0}/(2-s_0)}{jX_{m0} + jX_{lr0} + R_{r0}/(2-s_0)}\right).\end{aligned} \quad (3)$$

The terms R_0, X_0 are the equivalent zero-sequence parameters defined in terms of R_{s0}, R_{r0}, X_{m0}, X_{ls0}, and X_{lr0} which are stator resistance, rotor resistance, magnetizing reactance, stator leakage reactance, and rotor leakage reactance in zero-sequence circuit, respectively. It is worth noting that the zero-sequence parameters in Fig. 5(a) are not necessarily the same as those obtained from standard tests, since the stator–rotor coupling

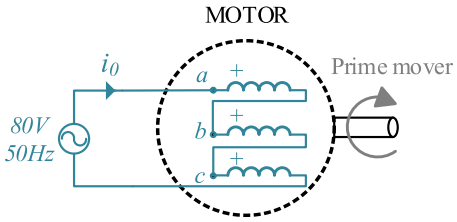

Fig. 6. Experimental configuration of a 3ph-IM for zero-sequence test.

through the third harmonics MMF is different from that of the fundamental MMF. Furthermore, the slip here, represented by s_0 in Fig. 5(a), is the relative slip of rotor with respect to the forward-rotating zero-sequence field, which can be defined as

$$s_0 = \frac{\omega_0 - \omega_r}{\omega_0} = 1 - 3\frac{\omega_r}{\omega_s} \tag{4}$$

where the ω_r is the rotor frequency.

At first glance, the complete evaluation of the parameters in this zero-sequence circuit seems to be tedious and would defeat the purpose of the proposed method. However, this is actually not the case here.

Using the rotor FOC method, even under post-fault operation, the difference between synchronous speed and rotor speed will generally not exceed the rated slip speed. This implies that even if the slip is up to 10%, it gives $0.9 < \omega_r/\omega_s < 1$ and from (4) the s_0 would be $-2 < s_0 < -1.7$.

Based on Fig. 5, as s_0 approaches –2, the rotor resistances in both the forward and backward branch will be very small, such that the current flowing into the magnetizing branch can be considered negligible. As a result, the forward branch impedance can be approximated as

$$Z_f = X_m/2 || (-R_{r0}/4 + jX_{lr0}/2) \approx -R_{r0}/4 + jX_{lr0}/2 \tag{5}$$

while the backward branch impedance can be approximated as

$$Z_b = X_m/2 || (R_{r0}/8 + jX_{lr0}/2) \approx R_{r0}/8 + jX_{lr0}/2. \tag{6}$$

The total zero-sequence impedance can then be given as

$$Z_0 = R_0 + jX_0 \approx (R_{s0} - R_{r0}/8) + j(X_{ls0} + X_{lr0}). \tag{7}$$

Based on this concept, R_0 and X_0 (or L_0) can be measured experimentally, as depicted in Fig. 6. A fixed voltage with a rated frequency 50 Hz should be applied to the machine with the three phases connected in series (exciting the zero-sequence circuit), while the rotor is rotated mechanically using an external prime mover (for e.g., using another motor), to a speed close to the synchronous speed. R_0 and X_0 can be calculated on a few points from the active power, reactive power, and current measured.

To better illustrate the estimation of R_0 and X_0, the data obtained through experimental tests are shown in Fig. 7. The values of R_0 and X_0 are calculated using the setup explained in Fig. 6, but with a few values of s_0. The results demonstrate that R_0 and X_0 are slip dependent; however, they are almost constant within typical operating region (marked as A in Fig. 7) where s_0 is approximately –2. The values obtained fit well with the characteristics predicted by (3), confirming the validity of the

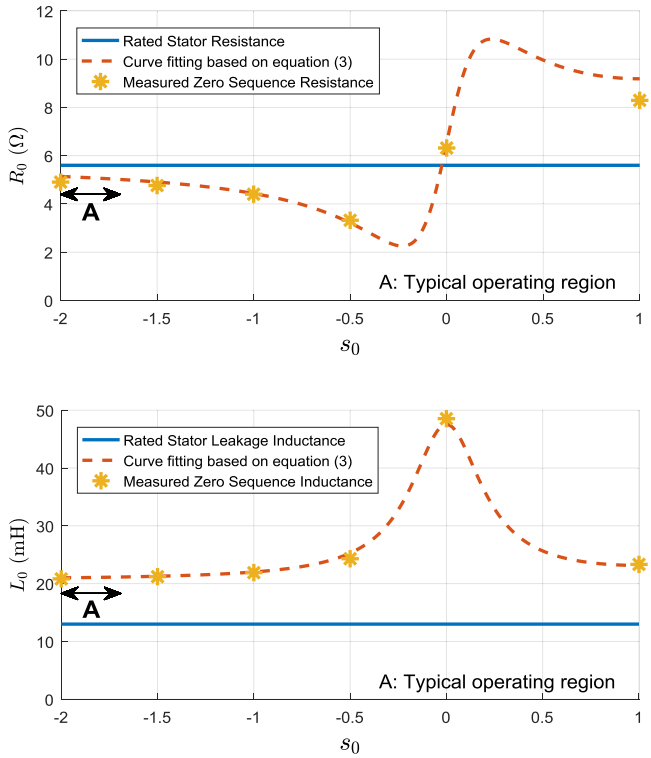

Fig. 7. Comparison of zero-sequence parameters of a 1-kW IM obtained from different approaches.

discussion. It should be highlighted that R_0 and X_0 values are different from the rated R_s and X_{ls}, as discussed earlier.

For the purpose of the proposed feedforward control, only the zero-sequence parameters around $s_0 = -2$ will be needed for the calculation, as will be explained in next section.

B. Zero-Sequence Voltage Calculation

With the zero-sequence current being predetermined by (1), the zero-sequence voltage can be estimated accordingly with the prior knowledge on zero-sequence parameters, i.e.,

$$V_0 = R_0 i_0 + L_0 \frac{d}{dt} i_0. \tag{8}$$

This, however, involves differentiating i_0 w.r.t time, which can be problematic since numerical differentiation of the current signal is susceptible to noise.

Based on Clarke transform, zero-sequence current can be expressed in terms of α–β currents instead of phase currents, as follows:

$$\begin{aligned} i_{0a} &= -i_\alpha \quad \text{(for fault on phase } a\text{)} \\ i_{0b} &= \frac{1}{2} i_\alpha - \frac{\sqrt{3}}{2} i_\beta \quad \text{(for fault on phase } b\text{)} \\ i_{0c} &= \frac{1}{2} i_\alpha + \frac{\sqrt{3}}{2} i_\beta \quad \text{(for fault on phase } c\text{)}. \end{aligned} \tag{9}$$

Taking advantage on the fact that α–β components are orthogonal, the time derivative of zero-sequence currents in (9)

can be obtained in terms of α–β current as follows:

$$\begin{aligned}\frac{d}{dt}i_{0a} &= \omega_s i_\beta \\ \frac{d}{dt}i_{0b} &= -\frac{\sqrt{3}}{2}\omega_s i_\alpha - \frac{1}{2}\omega_s i_\beta \\ \frac{d}{dt}i_{0c} &= \frac{\sqrt{3}}{2}\omega_s i_\alpha - \frac{1}{2}\omega_s i_\beta \end{aligned} \tag{10}$$

where ω_s is the synchronous frequency of the α–β currents. So, the numerical differentiation of the currents can be avoided.

By substituting (9) and (10) into (8), the zero-sequence voltage, for the fault in phase *a*, *b* or *c*, can be obtained as follows:

$$\begin{aligned} V_{0a} &= -R_0 i_\alpha + \omega_s L_0 i_\beta \\ V_{0b} &= \left(\frac{1}{2}R_0 - \frac{\sqrt{3}}{2}\omega_s L_0\right) i_\alpha + \left(-\frac{\sqrt{3}}{2}R_0 - \frac{1}{2}\omega_s L_0\right) i_\beta \\ V_{0c} &= \left(\frac{1}{2}R_0 + \frac{\sqrt{3}}{2}\omega_s L_0\right) i_\alpha + \left(\frac{\sqrt{3}}{2}R_0 - \frac{1}{2}\omega_s L_0\right) i_\beta . \end{aligned} \tag{11}$$

The zero-sequence parameters obtained previously together with α–β currents of the machine are enough to calculate the zero-sequence voltages of (11). Application of corresponding zero-sequence voltage terms into either topology given in Fig. 4 in a feedforward manner will allow the fault-tolerant control of the drive.

IV. Consideration of Inverter Nonlinearity

For an ideal inverter model depicted in Figs. 2 and 3 the inverter can be seen as a linear amplifier, i.e., the pole voltage output of the inverter is proportional to the control voltage or modulating signals. However, there are two important physical constraints which cause nonlinearity in the inverter, i.e.,

1) switching dead-time;
2) forward voltage drop of switches.

As a result, the actual inverter voltage will have slightly distorted. For a healthy motor, the magnitude of these distortion voltages is relatively small, and hence does not impose significant distortion onto the motor output torque. In fact, the effect of inverter nonlinearity would be, to a certain extent, compensated by the proportional part of the PI controllers in FOC.

However, this is not the case for the fault-tolerant control using 3 L-NCM and (3 + 1)L-NAL topologies. Due to the low *RL* values in zero-sequence circuit, the magnitude of the V_0 is relatively small and can be easily affected by the voltage error caused by aforementioned nonlinearity. Furthermore, this V_0 term has to be provided in feedforward manner without any feedback control loop.

A. Effect of Deadtime on Inverter Leg Voltage

The deadtime applied to a PWM signal delays the turn-ON instant of the inverter leg switches, shown in Fig. 8. Due to the conduction of freewheeling diodes during deadtime, it creates short error voltage pulses whose polarity depended on the polarity of the phase current. It has been demonstrated that the voltage error caused by deadtime can be sufficiently compensated by adding predefined voltage term into reference voltages prior to the PWM modulator [26]. The unique compensation term on each individual inverter leg is named $V^*_{\mathrm{DT}(k)}$ and is determined based on its current polarity sign(i_k), deadtime t_{dt} in second, and switching frequency f_{sw} as follows:

$$V^*_{\mathrm{DT}\,(k)} = \mathrm{sign}(i_k) t_{\mathrm{dt}} f_{\mathrm{sw}} V_{\mathrm{dc}} \quad (k : a, b, c, n). \tag{12}$$

The sign function in (12) detects the current polarity with a hysteresis band to reduce chattering effect around zero crossing point, i.e.,

$$\mathrm{sign}(i_k) = \begin{cases} 1 & i_k > +i_{\mathrm{th}} \\ 0 & -i_{\mathrm{th}} < i_k < +i_{\mathrm{th}} \\ -1 & i_k < -i_{\mathrm{th}} \end{cases} \tag{13}$$

where i_{th} is the hysteresis threshold that should be set to a relatively small value, for example, 0.05% of the motor-rated phase current. Synchronous current measurement at this point can further reduce the ripples of current reading and therefore achieve more accurate current polarity detection.

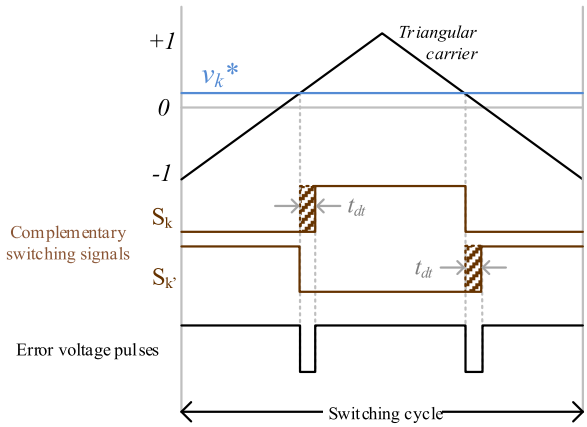

Fig. 8. Deadtime in the form of on-delay on PWM signals and propagated voltage error.

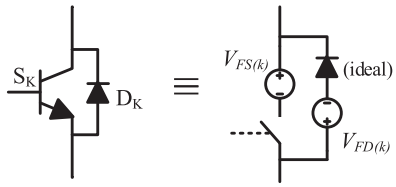

Fig. 9. Voltage model of inverter switch and recovery diode.

B. Effect of Switch Forward Voltage Drop

The on-state resistance, forward voltage, and junction temperature are the main factors that impact the total voltage drop on the conducting switch or recovery diode. However, all the factors involved can be lumped into a single voltage term in series with an ideal switch to represent the total voltage drop across the switch. The forward voltage model is shown in Fig. 9

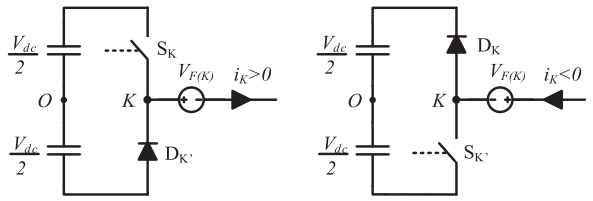

Fig. 10. Effect of on-state switch voltage drop as a function of current polarity on inverter leg.

as $V_{FS(K)}$ for semiconductor switch and $V_{FD(K)}$ for recovery diode.

Depending on the choice of component, the voltage drop across the insulated-gate bipolar transistor (IGBT) and its recovery diode might be slightly different. For simplicity, the two terms can be assumed to be equal here

$$V_{FS(k)} = V_{FD(k)} = V_{F(k)}(k : a, b, c, n). \tag{14}$$

As long as the current direction is positive, either top switch or bottom diode would be forward conducting. In this situation, the voltage drop on both switch and diode will have the same polarity and can be realized as a constant bias voltage to the inverter pole voltage, as shown in Fig. 10. Similarly, the polarity of biasing voltage will be reversed for negative current. Since the current polarity is determined using (13), the semiconductor voltage drop can be compensated too. The compensation term which is a function of current polarity and semiconductor forward voltage should be added to the reference voltage in a feedforward fashion. The generic form of compensation term here is

$$V^*_{F(k)} = \text{sign}(i_k)V_{F(k)}(k : a, b, c, n) \tag{15}$$

where $V_{F(K)}$ is total normalized voltage drop on *k*th leg semiconductors and is obtained from switch datasheet.

V. Fault-Tolerant Field-Oriented Controller

The proposed fault-tolerant controller is aimed to maintain the FOC even in post-fault mode without any interference to the controller. So, the modifications on controller output required for each post-fault topology in Fig. 1 are explained separately.

1) There is no change to the controller if the (3 + 1)L-PAL topology is used since the faulted inverter leg is replaced with auxiliary leg.
2) For the PCM configuration, the open-leg inverter fault is compensated by clamping the corresponding motor terminal to the capacitor midpoint. Therefore, the modulating signal of the failed leg should be deducted from the other two active inverter legs only [27].
3) For the cases in which two motor phases are involved in post-fault mode, the consequence of fault and reconfiguration is going to be tolerated by adding compensation V_0 term for the 3 L-NCM and (3 + 1)L-NAL configurations, as discussed in (11). This zero-sequence voltage is going to be applied to the motor in post-fault mode in a feedforward manner in accordance with topologies in Fig. 4.

The effect of inverter nonlinearity must be compensated for all cases, in the form of a square-wave signal added to the modulating index. The post-fault topologies with two stator phases involved, i.e., 3 L-NCM and (3 + 1)L-NAL, are the main scope of this study because of having crucial situation. Based on that, a unified feedforward module is added to typical FOC drive and the overall schematic of fault-tolerant filed oriented drive is given in Fig. 11. However, minor modifications need to be applied on the modulating signals for 3 L-PCM and (3 + 1)L-PAL configurations [27]; hence, it can be included in unified feedforward module to tolerate the fault in all available configurations.

The inputs to unified feedforward module shown in Fig. 11 are the modulating index produced by FOC, V_0 corresponding to the fault type, and inverter nonlinearity compensation terms.

By activating switches in accordance with status of the drive, the modifications will be applied to the modulating index before SPWM stage. The switch activation commands for each fault type, fault location and post-fault topology is given in Table I in encoded format. With this configuration, one or two out of four switches per modulating signal shown in Fig. 12 would be active at different situations.

Based on the commands in Table I, for instance, the modulating signals in post-fault mode for 3 L-NCM would be modified to be

$$\begin{matrix} G_a = 2 \\ G_b = 1 \\ G_c = 1 \end{matrix} \rightarrow \begin{vmatrix} \hat{v}^*_a = N.A.(\text{open circuit}) \\ \hat{v}^*_b = v^*_b - V_{0a} + V_{DTb} + V_{Fb} \\ \hat{v}^*_c = v^*_c - V_{0a} + V_{DTc} + V_{Fc} \end{vmatrix}$$

and for (3 + 1)L-NAL is

$$\begin{matrix} G_a = 4 \\ G_b = 1 \\ G_c = 1 \end{matrix} \rightarrow \begin{vmatrix} \hat{v}^*_a = V_{0a} + V_{DTn} + V_{Fn} \\ \hat{v}^*_b = v^*_b + V_{DTb} + V_{Fb} \\ \hat{v}^*_c = v^*_c + V_{DTc} + V_{Fc}. \end{vmatrix}$$

Note that $\hat{v}^*_a$ of (3 + 1)L-NAL configuration is used as modulating index for auxiliary (neutral) leg.

VI. Results and Discussions

The simulation and experimental verification of the proposed methods are conducted on a 1-kW squirrel cage IM drive with machine parameters stated in Table II. In both simulation and experiment, the SPWM with 5-kHz triangular carrier is implemented. A 5-kW three-leg IGBT inverter powered from dc supply (TDK-Lambda GEN600-8.5) comes with split capacitors, 2200 μF each in experiment. The load is inserted mechanically by coupling the motor shaft to a permanent magnet synchronous generator feeding adjustable resistor. The controller is executed in dSPACE DS1104 platform along with current and rotor speed feedback. The three-phase currents are synchronously measured at beginning of each PWM cycle.

The test rig for this study is shown in Fig. 13. For all the test, the reference i_{ds} is fixed to 1.8 A and the reference speed is decided to be 1400 r/min for healthy and post-fault operation. A constant load would be applied to the motor shaft as long as the speed is maintained constant. The detection and discrimination of the fault could be done by comparing certain residual signal [30], monitoring of the zero-sequence voltage with respect to

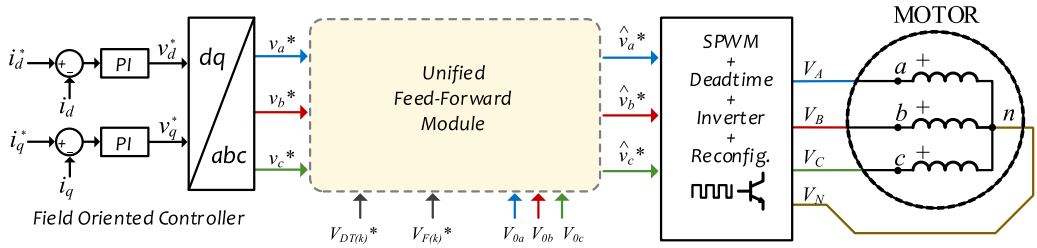

Fig. 11. Overall structure of fault-tolerant field-oriented 3ph-IM drive.

TABLE I
SWITCH ACTIVATION COMMANDS FOR UNIFIED FEEDFORWARD MODULE

Faulted Phase/Leg	'a'			'b'			'c'		
	G_a	G_b	G_c	G_a	G_b	G_c	G_a	G_b	G_c
Healthy	1	1	1	1	1	1	1	1	1
NCM	2	1	1	1	2	1	1	1	2
NAL	4	1	1	1	4	1	1	1	4

$(G_k)10 = (G_{k3}G_{k2}G_{k1})_2 \quad k : a, b, c.$

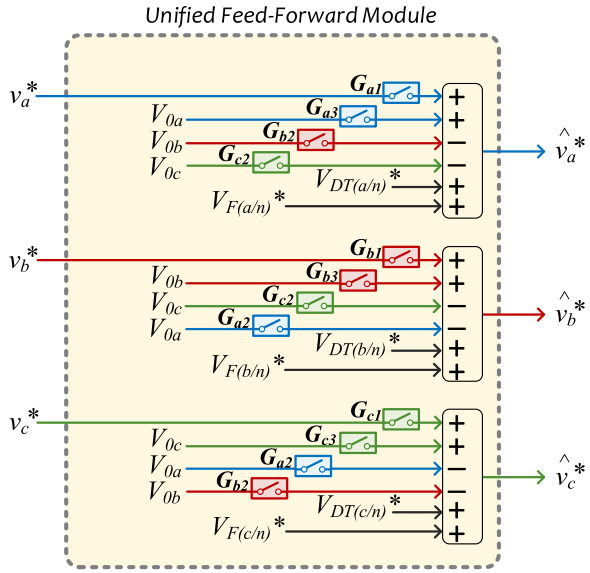

Fig. 12. Modulating index modifications in unified feedforward module.

TABLE II
IM RATED VALUES AND PARAMETERS

Rated Power	1000 W	*Stator Resistance (AC)*	5.6 Ω
Rated Phase Voltage	220 V	*Stator Resistance (DC)*	5.08 Ω
Rated Phase Current	2.7 A	*Rotor Resistance*	5.9 Ω
Rated Speed	2800 min^{-1}	*Stator Leakage Inductance*	13 mH
Rated Frequency	50 Hz	*Rotor Leakage Inductance*	13 mH
		Magnetizing Inductance	426 mH
		Zero sequence Resistance	4.8 Ω
		Zero sequence Inductance	21 mH

the neutral point of the stator winding [31] or current signature in *dq* plane [32]. Since the contribution of this work focuses on the control method, the authors are assuming that previous methods for fault detection [30]–[32], particularly OPF, can be readily applicable. The connecting devices reconfigure the drive after detection and clearance of the fault.

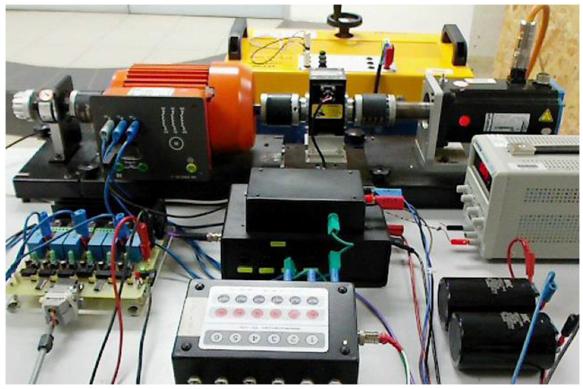

Fig. 13. Test rig of fault-tolerant drive.

The controller modifications will be applied onto the controller once the drive is reconfigured. In the experiment for this work, two relays are incorporated in the test rig to open/close the connection between inverter and motor terminals. These connecting devices are meant to emulate the OPF on the drive and then reconfigure it to post-fault topology for both simulation and experiment.

A. Fault-Tolerant Operation

The experimental results for the 3 L-NCM and (3 + 1)L-NAL configurations are shown in Figs. 14 and 15, respectively. The normalized modulating index, phase current, torque, and speed are shown for both simulation and experiment side by side.

Initially, the drive operates in healthy mode. At $t = 0.2$ s, an OPF is created by disconnecting phase "*a*" of the machine using a relay (in fault emulator box). Due to the fault, the machine is reduced to a single-phase machine, as evident from the fact that the phase "*b*" and "*c*" currents are equal and opposite, i.e., $i_b = -i_c$. As expected, severe torque oscillations appear, causing the speed to oscillate as well.

To simulate the actual time needed to faultsuppressed detection and reconfiguration, a delay of 0.1 s is allowed before the neutral of the motor is connected to the dc-link midpoint for 3 L-NCM, or to an auxiliary inverter leg for the case of (3 + 1)L-NAL. Compensation voltage of V_0 is injected together with the reconfiguration at $t = 0.3$ s, based on the method described in Section V. As visible from Figs. 14 and 15, the injection of feedforward compensation voltage effectively has reduced the torque and speed oscillations. However, the oscillations were not fully suppressed.

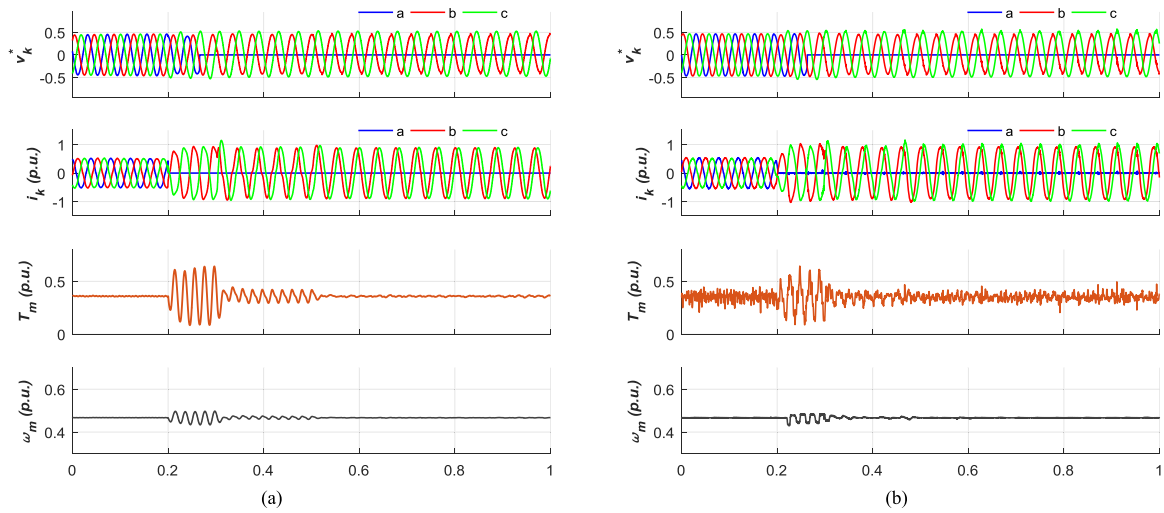

Fig. 14. Simulation and experimental results for 3 L-NCM post-fault topology. (a) Simulation results. (b) Experimental results.

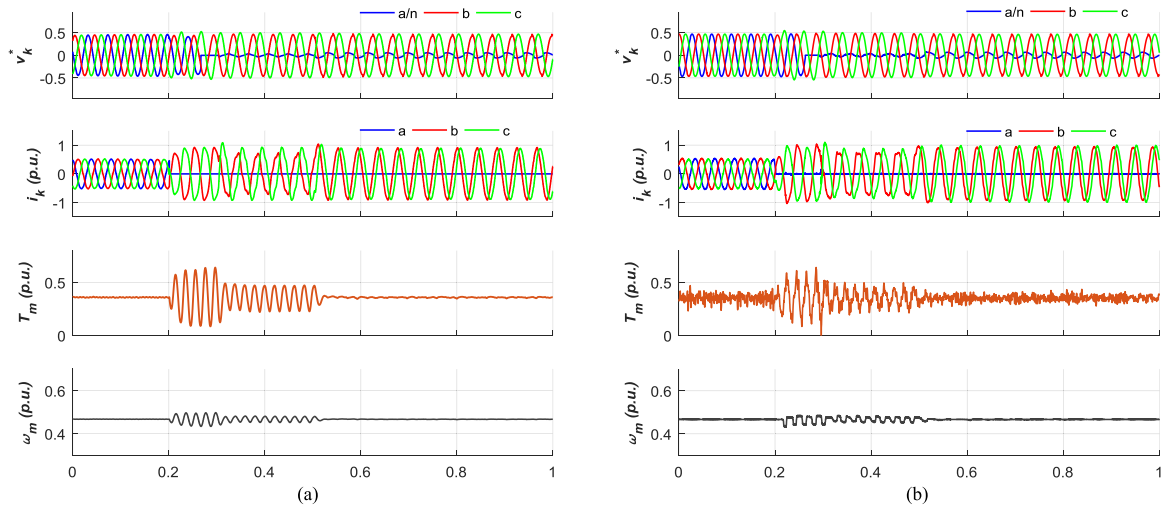

Fig. 15. Simulation and experimental results for (3 + 1)L-NAL post-fault topology. (a) Simulation results. (b) Experimental results.

At $t = 0.5$ s, the inverter nonlinearity compensation was activated, where deadtime and forward voltage compensation terms were added to the modulating index. It changes the shape of modulating signals being like "broken sine waves" as shown in Fig. 16. Significant reduction in torque and speed oscillations can be observed from this point onwards, confirming the importance of these compensation.

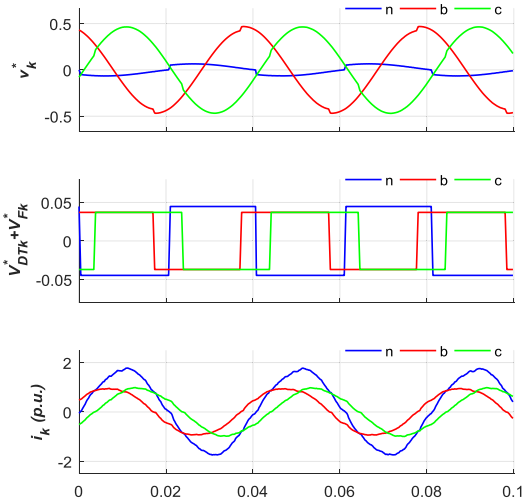

Fig. 16. Modulating index, inverter nonlinearity compensation terms and inverter leg currents of (3 + 1)L-NAL configuration on experimental results.

B. Post-Fault Self-Start

By maintaining the FOC even in the presence of fault, the faulted drive is able to self-start like a healthy drive in post-fault mode since torque and flux currents are maintained. The comparison of healthy and post-fault self-start capability in experiment is shown in Fig. 17. The results demonstrated that the steady-state torque response of the faulted drives in Fig. 17(b) and(c) are fast and close enough to the healthy drive in Fig. 17(a), with slightly higher ripples. The transient and steady-state peak

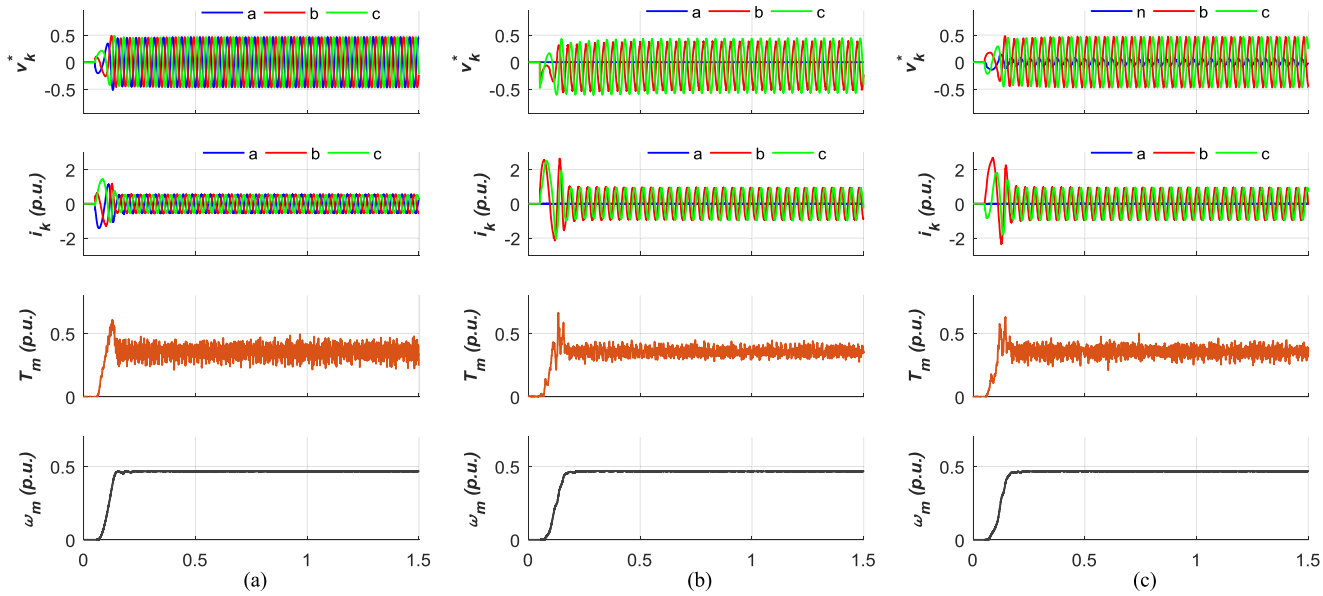

Fig. 17. Experimental results showing the self-start performance of (a) healthy drive and post-fault, (b) 3 L-NCM, and (c) (3 + 1)L-NAL topology.

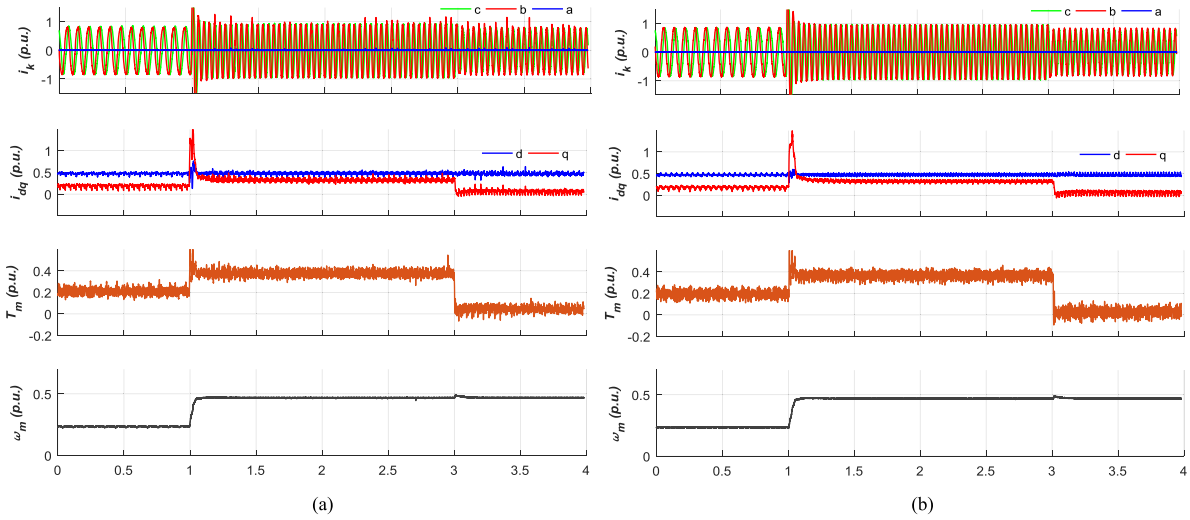

Fig. 18. Experimental results showing the dynamic performance of (a) 3 L-NCM and (b) (3 + 1)L-NAL topology.

phase current of the faulted drives are $\sqrt{3}$ times bigger than healthy drive as expected.

C. Post-Fault Dynamic Response

The dynamic performance of the control method was also evaluated by introducing step change in speed and load torque as shown in Fig. 18. For both the 3 L-NCM and (3 + 1)L-NAL cases, the speed was stepped from 700 to 1400 r/min at $t = 1$ s, followed by a step change in load (from 0.4 p.u. to no load) at $t = 3$ s. The step change in speed is done by stepping the speed reference in ControlDesk. It should be highlighted that since the motor is coupled to a permanent magnet generator with fixed resistive load (acting as mechanical load), increasing the speed increases the generator's voltage which causes the load torque to increase. Later, the step change in load is done by disconnecting the load resistors of the permanent magnet generator using relays. As visible from the figure, the proposed control method was able to regulate the speed as well as the currents as one would expect from a functioning field-oriented-controlled motor.

VII. Conclusion

In this study, a new fault-tolerant scheme has been proposed to be embedded into typical FOC drives. A simple method is proposed where fault-tolerant FOC can be achieved with minimal modification, by injecting suitable zero-sequence voltage to the faulted motor in feedforward fashion. Since feedforward method is used, it is important to obtain the correct zero-sequence circuit parameters to compute the required zero-sequence voltage. These are highlighted and explained in this paper.

Furthermore, the significance of the inverter nonlinearities in post-fault configuration is investigated by taking into account the effect of deadtime and forward voltage drop on the inverter

switches. By applying the zero-sequence voltage to the motor along with the compensation of the inverter nonlinearities, the faulted drive is controlled sufficiently to continue operation in post-fault mode. The highlighted findings out of this study are as follows.

1) The proposed control method based on the zero-sequence voltage introduces an efficient way to control the faulted drive, avoiding the complexity of calculating back electromotive force voltage through magnetizing inductance.
2) The characteristics of zero-sequence circuit has been discussed and the method to obtain the required zero-sequence parameter was explained.
3) It is shown that the inverter nonlinearity makes a significant impact on the performance of the fault-tolerant controller in post-fault mode which has been neglected and could to be compensated.
4) The generality of this fault-tolerant control method allows easy adoption in different fault-tolerant FOC drive with minor modifications. Successful implementation of the proposed control method on 3 L- NCM and (3 + 1)L-NAL topologies has been demonstrated in this paper.
5) The self-start capability and the dynamic performance of the proposed fault-tolerant drive for both 3 L-NCM and (3 + 1)L-NAL configurations are confirmed as it maintains the FOC to control over torque and flux producing currents.

REFERENCES

[1] H. W. Van der Broeck and J. D. Van Wyk, "A comparative investigation of a three-phase induction machine drive with a component minimized voltage-fed inverter under diferent control options," *IEEE Trans. Ind. Appl.*, vol. IA-20, no. 2, pp. 309–320, Mar. 1984.

[2] T. A. Lipo, "A strategy for improving reliability of field-oriented controlled induction motor drives," *IEEE Trans. Ind. Appl.*, vol. 29, no. 5, pp. 910–918, Sep./Oct. 1993.

[3] F. Blaabjerg, D. O. Neacsu, and J. K. Pedersen, "Adaptive SVM to compensate dc-link voltage ripple for four-switch three-phase voltage-source inverters," *IEEE Trans. Power Electron.*, vol. 14, no. 4, pp. 743–752, Jul. 1999.

[4] F. Blaabjerg, S. Freysson, H. H. Hansen, and S. Hansen, "A new optimized space vector modulation strategy for a component minimized voltage source inverter," *IEEE Trans. Power Electron.*, vol. 12, no. 4, pp. 704–714, Jul. 1997.

[5] R. Wang, J. Zhao, and Y. Liu, "A comprehensive investigation of four-switch three-phase voltage source inverter based on double Fourier integral analysis," *IEEE Trans. Power Electron.*, vol. 26, no. 10, pp. 2774–2787, Oct. 2011.

[6] Y. Song and B. Wang, "Analysis and experimental verification of a fault-tolerant HEV powertrain," *IEEE Trans. Power Electron.*, vol. 28, no. 12, pp. 5854–5864, Dec. 2013.

[7] P. Garg, S. Essakiappan, H. S. Krishnamoorthy, and P. N. Enjeti, "A fault-tolerant three-phase adjustable speed drive topology with active common-mode voltage suppression," *IEEE Trans. Power Electron.*, vol. 30, no. 5, pp. 2828–2839, May 2015.

[8] C. Zhu, Z. Zeng, and R. Zhao, "Comprehensive analysis and reduction of torque ripples in three-phase four-switch inverter-fed PMSM drives using space vector pulse-width modulation," *IEEE Trans. Power Electron.*, vol. 32, no. 7, pp. 5411–5424, Jul. 2017.

[9] R. R. Errabelli and P. Mutschler, "Fault-tolerant voltage source inverter for permanent magnet drives," *IEEE Trans. Power Electron.*, vol. 27, no. 2, pp. 500–508, Feb. 2012.

[10] S. Bolognani, M. Zordan, and M. Zigliotto, "Experimental faul-tolerant control of {PMSM} drive," *IEEE Trans. Ind. Electron.*, vol. 47, no. 5, pp. 1134–1141, Oct. 2000.

[11] N. Bianchi, S. Bolognani, M. Zigliotto, and M. Zordan, "Innovative remedial strategies for inverter faults in IPM synchronous motor drives," *IEEE Trans. Energy Convers.*, vol. 18, no. 2, pp. 306–314, Jun. 2003.

[12] M. Beltrao de Rossiter Correa, C. B. Jacobina, E. R. Cabral da Silva, and A. M. N. Lima, "An induction motor drive system with improved fault tolerance," *IEEE Trans. Ind. Appl.*, vol. 37, no. 3, pp. 873–879, May/Jun. 2001.

[13] A. Gaeta, G. Scelba, and A. Consoli, "Modeling and control of three-phase PMSMs under open-phase fault," *IEEE Trans. Ind. Appl.*, vol. 49, no. 1, pp. 74–83, Jan./Feb. 2013.

[14] O. Wallmark, L. Harnefors, and O. Carlson, "Control algorithms for a fault-tolerant PMSM drive," *IEEE Trans. Ind. Electron.*, vol. 54, no. 4, pp. 1973–1980, Aug. 2007.

[15] A. Sayed-Ahmed, B. Mirafzal, and N. A. O. Demerdash, "Fault-tolerant technique for Δ-connected AC-motor drives," *IEEE Trans. Energy Convers.*, vol. 26, no. 2, pp. 646–653, Jun. 2011.

[16] A. Boglietti, R. Bojoi, A. Cavagnino, and A. Tenconi, "Efficiency analysis of PWM inverter fed three-phase and dual three-phase high frequency induction machines for low/medium power applications," *IEEE Trans. Ind. Electron.*, vol. 55, no. 5, pp. 2015–2023, May 2008.

[17] J. A. Restrepo, A. Berzoy, A. E. Ginart, J. M. Aller, R. G. Harley, and T. G. Habetler, "Switching strategies for fault tolerant operation of single DC-link dual converters," *IEEE Trans. Power Electron.*, vol. 27, no. 2, pp. 509–518, Feb. 2012.

[18] E. Levi, "Advances in converter control and innovative exploitation of additional degrees of freedom for multiphase machines," *IEEE Trans. Ind. Electron.*, vol. 63, no. 1, pp. 433–448, Jan. 2016.

[19] H. S. Che, M. J. Duran, E. Levi, M. Jones, W. P. Hew, and N. A. Rahim, "Postfault operation of an asymmetrical six-phase induction machine with single and two isolated neutral points," *IEEE Trans. Power Electron.*, vol. 29, no. 10, pp. 5406–5416, Oct. 2014.

[20] W. N. W. A. Munim, M. J. Duran, H. S. Che, M. Bermudez, I. Gonzalez-Prieto, and N. A. Rahim, "A unified analysis of the fault tolerance capability in six-phase induction motor drives," *IEEE Trans. Power Electron.*, vol. 32, no. 10, pp. 7834–7836, Oct. 2017.

[21] A. S. Abdel-Khalik, M. S. Hamad, A. M. Massoud, and S. Ahmed, "Post-fault operation of a nine-phase six-terminal induction machine under single open-line fault," *IEEE Trans. Ind. Electron.*, vol. 65, no. 2, pp. 1084–1096, Feb. 2018.

[22] M. Tousizadeh, H. S. Che, J. Selvaraj, N. A. Rahim, and B.-T. Ooi, "Performance comparison of fault-tolerant three-phase induction motor drives considering current and voltage limits," *IEEE Trans. Ind. Electron. Electron.*, vol. 66, no. 4, pp. 2639–2648, Apr. 2019.

[23] P. Krause, O. Wasynczuk, S. D. Sudhoff, and S. Pekarek, *Analysis of Electrical Machinery and Drives*. Piscataway, NJ, USA: IEEE Press, 2013.

[24] J. E. Brown and O. I. Butler, "The zero-sequence parameters and performance of three-phase induction motors," *Proc. IEE—Part IV, Inst. Monogr.*, vol. 101, no. 7, pp. 219–224, 1954.

[25] C. Grantham, "Zero-sequence dynamic braking and parameter determination," *IEE Proc. B—Elect. Power Appl.*, vol. 130, no. 6, pp. 392–398, 1983.

[26] I. R. Bojoi, *Analysis, Design and Implementation of a Dual Three-Phase Vector Controlled Induction Motor Drive*, Turin, Italy: Politecnico Di Torino, 2002.

[27] R. L. de Araujo Ribeiro, C. B. Jacobina, E. R. C. da Silva, and A. M. N. Lima, "Fault-tolerant voltage-fed PWM inverter AC motor drive systems," *IEEE Trans. Ind. Electron.*, vol. 51, no. 2, pp. 439–446, Apr. 2004.

[28] K. Ni, W. Li, Y. Liu, D. Yu, and Y. Hu, "Phase current reconstruction for the grid-side converter with four-switch three-phase topology in a DFIG-WT," *IEEE Access*, vol. 6, pp. 39287 39297, Jul. 2018.

[29] W. Sae-Kok, D. M. Grant, and B. W. Williams, "System reconfiguration under open-switch faults in a doubly fed induction machine," *IET Renewable Power Gener.*, vol. 4, no. 5, pp. 458–470, 2010.

[30] Q. T. An, L. Sun, and L. Z. Sun, "Current residual vector-based open-switch fault diagnosis of inverters in PMSM drive systems," *IEEE Trans. Power Electron.*, vol. 30, no. 5, pp. 2814–2827, May 2015.

[31] J. Hang, J. Zhang, and M. Cheng, "Detection and discrimination of open phase fault in permanent magnet synchronous motor drive system," *IEEE Trans. Power Electron.*, vol. 31, no. 7, pp. 4697–4709, Jul. 2016.

[32] S. S. Kuruppu and N. A. Kulatunga, "D-Q current signature-based faulted phase localization for SM-PMAC machine drives," *IEEE Trans. Ind. Electron.*, vol. 62, no. 1, pp. 113–121, Jan. 2015.

Mahdi Tousizadeh was born in Isfahan, Iran. He received the B.Eng. degree in electrical engineering power from Islamic Azad University, Isfahan, Iran, in 2009, and the M.Eng. degree in electrical engineering–mechatronics and automatic control from University Technology Malaysia, Skudai, Malaysia, in 2012. He is currently working toward the Ph.D. degree in electrical engineering–motor drive at the University of Malaya, Kuala Lumpur, Malaysia.

He has been a Researcher with UM Power Energy Dedicated Advanced Centre, University of Malaya, since 2013. His research interests include fault-tolerant control of machines and drives as well as power electronics converters for electric vehicle applications.

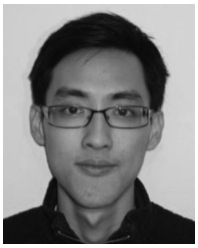

Hang Seng Che (M'14) received the B.Eng. degree in electrical engineering from the University of Malaya, Kuala Lumpur, Malaysia, in 2009, and the Ph.D. degree in electrical engineering under the auspices of a dual Ph.D. program between the University of Malaya and Liverpool John Moores University, Liverpool, U.K., in 2013.

Since 2013, he has been with UM Power Energy Dedicate d' Advanced Centre, University of Malaya, where he is currently a Senior Lecturer. His research interests include multiphase machines and drives, fault-tolerant control, and power electronics converters for renewable energy applications.

Dr. Che has been an Associate Editor for the *IET Electric Power Applications* journal since 2016. He was the recipient of the 2009 Kuok Foundation Postgraduate Scholarship Award for his Ph.D. study.

Jeyraj Selvaraj received the B.Eng. (Hons.) degree in electrical engineering from Multimedia University Cyberjaya, Cyberjaya, Malaysia, in 2002, the M.Sc. degree in power electronics and drives jointly from the University of Birmingham, Birmingham, U.K., and the University of Nottingham, Nottingham, U.K., in 2004, and the Ph.D. degree in electrical engineering from the University of Malaya, Kuala Lumpur, Malaysia, in 2009.

He is currently an Associate Professor and the Deputy Director with the University of Malaya Power Energy Dedicated Advanced Centre, University of Malaya. His research interests include solar system, single- and three-phase multilevel inverters, digital current-control techniques, photovoltaic inverters, and dc–dc converters.

Dr. Selvaraj is also a member of working group on solar photovoltaic system in Malaysia. He was one of the recipients of the NAM Research Training Fellowship for Young Scientist in 2016.

Nasrudin Abd Rahim (M'80–SM'08) received the B.Sc. (Hons.) degree, the B.Eng. degree in electrical electronic engineering, and the M.Sc. degree in electrical power engineering from the University of Strathclyde, Glasgow, U.K., and the Ph.D. degree in power electronics from Heriot–Watt University, Edinburgh, U.K., in 1995.

He is currently a Professor with the University of Malaya, Kuala Lumpur, Malaysia, where he is also the Director of the UM Power Energy Dedicated Advanced Centre. His research interests include power electronics, solar PV and wind technologies, real-time control systems, and electrical drives.

Dr. Rahim is a fellow of the Institution of Engineering and Technology, U.K., and the Academy of Sciences Malaysia. He is also a Professional Engineer (Malaysia) and a Chartered Engineer (U.K).

Boon-Teck Ooi (S'69–M'71–SM'85–F'02–LF'05) was born in Kuala Lumpur, Malaysia. He received the B.Eng. (Hons.) degree from the University of Adelaide, Adelaide, SA, Australia, in 1962, the M.S. degree from the Massachusetts Institute of Technology, Cambridge, MA, USA, in 1967, and the Ph.D. degree from McGill University, Montreal, QC, Canada in 1970, all in electrical engineering.

He is currently an Emeritus Professor with the Department of Electrical and Computer Engineering, McGill University. He is currently a Visiting Professor with the University of Malaya, Kuala Lumpur, Malaysia, University of Adelaide, and Nanyang University of Technology, Singapore. His research has been in power electronics: unity power factor PWM rectifiers, the voltage-source converter family of HVdc, multiterminal VSC-HVdc, controllers for flexible ac transmission systems, power quality and distributed generation, MMC, multiterminal MMC HVdc, and dc–dc converters. In renewable energy technologies, his research has been in wind turbine-generators, doubly fed induction motors, impact of wind power on grid frequency, and islanded wind farms.